

Interannual modulation of subthermocline eddy kinetic energy east of the Philippines

Yuchao Hui¹, Linlin Zhang², Zhenxiao Wang¹, Fan WANG², and Dunxin Hu³

¹Institute of Oceanology Chinese Academy of Sciences

²Institute of Oceanology, Chinese Academy of Sciences

³IOCAS

November 22, 2022

Abstract

Interannual variation of subthermocline eddy kinetic energy (EKE) east of the Philippines is investigated based on mooring measurements during 2015-2019 and ocean state estimates during 1995-2017 from the Oceanic General Circulation Model for the Earth Simulator (OFES). Prominent interannual variation of EKE is detected below the thermocline east of the Philippine coast, which is closely related to the El Niño and Southern Oscillation (ENSO) events and generally lags the Nino3.4 index by 14 months. Further energy diagnostic analysis indicates that the interannual variation of subthermocline EKE is controlled by both baroclinic and barotropic instability of the background flows and dominated by the barotropic instability especially. Barotropic instability in the southern part of the Philippine coast is associated with the subsurface component of the quasi-permanent anticyclonic eddy Halmahera Eddy (HE), while that in the northern part is closely related to the Mindanao Undercurrent (MUC). Both HE and MUC are modulated by the ENSO events. When El Niño occurs, negative sea surface height anomalies appear near the dateline and propagate westward in the form of the first mode baroclinic Rossby wave, exerting delayed impacts upon the western boundary currents east of the Philippine coast and further modulating the interannual variation of subthermocline EKE. Moreover, the barotropic energy conversion rate and its corresponding subthermocline EKE at lower latitudes responds relatively faster to ENSO due to the higher Rossby wave phase speed there.

Hosted file

interannual_modulation_subeke_submit.doc available at <https://authorea.com/users/536235/articles/598994-interannual-modulation-of-subthermocline-eddy-kinetic-energy-east-of-the-philippines>

28 **Abstract**

29 Interannual variation of subthermocline eddy kinetic energy (EKE) east of the Philippines is
30 investigated based on mooring measurements during 2015-2019 and ocean state estimates during
31 1995-2017 from the Oceanic General Circulation Model for the Earth Simulator (OFES).
32 Prominent interannual variation of EKE is detected below the thermocline east of the Philippine
33 coast, which is closely related to the El Niño and Southern Oscillation (ENSO) events and
34 generally lags the Nino3.4 index by 14 months. Further energy diagnostic analysis indicates that
35 the interannual variation of subthermocline EKE is controlled by both baroclinic and barotropic
36 instability of the background flows and dominated by the barotropic instability especially.
37 Barotropic instability in the southern part of the Philippine coast is associated with the subsurface
38 component of the quasi-permanent anticyclonic eddy Halmahera Eddy (HE), while that in the
39 northern part is closely related to the Mindanao Undercurrent (MUC). Both HE and MUC are
40 modulated by the ENSO events. When El Niño occurs, negative sea surface height anomalies
41 appear near the dateline and propagate westward in the form of the first mode baroclinic Rossby
42 wave, exerting delayed impacts upon the western boundary currents east of the Philippine coast
43 and further modulating the interannual variation of subthermocline EKE. Moreover, the
44 barotropic energy conversion rate and its corresponding subthermocline EKE at lower latitudes
45 responds relatively faster to ENSO due to the higher Rossby wave phase speed there.

46

47 **Plain Language Summary**

48 Subthermocline meso-scale eddies with maximum velocity below the thermocline are
49 distributed widely over the world oceans and play a crucial role in the transport of subsurface

50 waters. The region east of the Philippine coast is featured with energetic eddies and high EKE in
51 the subsurface layer. These eddies are intrinsic to the ocean, and extract energy from the mean
52 potential energy and mean kinetic energy of the background currents. Based on 4-year mooring
53 measurements and OFES outputs during 1995-2017, strong interannual variation of
54 subthermocline EKE is detected in this region. Further analysis demonstrates that this interannual
55 variation is mainly modulated by the evolution of barotropic instability, which is associated with
56 the background flows of MUC and HE east of the Philippine coast. Additionally, the interannual
57 variation of subthermocline EKE seems to be influenced by ENSO. The wind stress curl anomaly
58 associated with El Niño events excites negative sea surface anomaly (SSHA) near the dateline,
59 and the SSHA propagates westward in the first mode Rossby waves, producing delayed impacts
60 on the western boundary currents and then on the variation of subthermocline EKE. This work
61 enriches our knowledge of the low-frequency modulation of subthermocline EKE in this region.

62

63 **Keywords**

64 subthermocline EKE; interannual variation; western tropical Pacific; baroclinic\barotropic
65 instability

66

67 **1. Introduction**

68 Meso-scale eddies are ubiquitous in the global ocean, which play crucial roles in modulating the
69 variability of ocean currents, the cycle of material and energy, and even the climate change (e.g.,
70 Stammer 1998; Fu 2009; Chelton et al. 2011a). Generally, mesoscale eddies can be divided into
71 two categories: surface-intensified eddy that has maximum velocity core in the upper layer and is

72 easily captured by sea surface features (e.g. Chelton et al. 2011b; Faghmous et al. 2015), and
73 subthermocline eddy that mainly exists below the thermocline and shows very weak or even no
74 signals at the sea surface (e.g. Mc Williams, 1985; Assassi et al., 2016). Due to the difficulty in
75 observing, there are relatively few studies on subthermocline eddies. These limited studies
76 indicate that subthermocline eddies are distributed widely over the world oceans and play an
77 essential role in the transport of water mass below the thermocline (e.g. Simpson and Lynn 1990;
78 Shapiro and Meschanov 1991; Richardson et al. 2000; Johnson and McTaggart 2010; Chiang et
79 al. 2015; Nan et al. 2017).

80 The western tropical Pacific is the ‘crossroad’ of currents from the northern and southern
81 hemispheres, and is featured with a complex three-dimensional circulation system. In the upper
82 layer, North Equatorial Current (NEC) flows westward and bifurcates into northward Kuroshio
83 and southward Mindanao Current (MC) when impinging at the Philippine coast at about 14°N
84 (e.g. Nitani 1972; Toole et al. 1990; Lukas et al. 1996; Hu et al. 2015). Further south, the main
85 body of MC that turns to the east combines with the New Guinea Coastal Current/Undercurrent
86 (NGCC/NGCUC) forming the source region of eastward-flowing North Equatorial Counter
87 Current (NECC) (Lukas et al. 1991). Below the surface circulation system, opposite subsurface
88 undercurrents appear, such as the Mindanao Undercurrent (MUC), Luzon Undercurrent (LUC),
89 North Equatorial Undercurrent (NEUC), and North Equatorial Subsurface Current (NESC) (Fig.
90 1; e.g., Hu and Cui 1989; Yuan et al. 2014; Qiu et al. 2013; Wang et al., 2015; Hu et al. 2020).

91 The complicated surface and subsurface current system in the western tropical Pacific provide
92 advantageous conditions for the generation of subthermocline eddies. Early hydrographic
93 observations have shown the hints of subthermocline eddies existing east of the Philippine coast

94 (e.g., Firing et al., 2005; Dutrieux 2009). Recent enhanced mooring measurements also reveal
95 significant intraseasonal variations of velocity with a period of 60-120 days centering below the
96 thermocline, and these intraseasonal signals are attributed to the activity of subthermocline
97 eddies (e.g., Zhang et al. 2014; Wang et al. 2014). Meanwhile, investigations based on model
98 outputs demonstrate that abundant subthermocline eddies and high eddy kinetic energy (EKE)
99 appear in this region (Fig. 2; e.g., Qu et al. 2012; Chiang and Qu, 2013; Xu et al. 2019). These
100 eddies are believed to be intrinsic to the ocean, and both barotropic and baroclinic instability are
101 important in the generation of these eddies (Dutrieux 2009; Chiang and Qu 2013; Wang et al.
102 2014; Chiang et al. 2015).

103 However, due to the lack of long-time observations focusing on subthermocline eddies in this
104 region, most of previous studies tend to concentrate on the statistical characteristics, and only a
105 few studies pay attention to the temporal variation of subthermocline eddies and their associated
106 EKE. Based on 4 years of mooring observations and OFES outputs, Zhang et al. (2021) reveals
107 the seasonal cycle of subthermocline EKE east of the Philippine coast. On the interannual time
108 scale, basin-wide wind stress anomalies associated with El Niño and Southern Oscillation
109 (ENSO) significantly modulate the variation of currents in the western Pacific through Ekman
110 and Rossby wave dynamics (e.g., Kashino et al. 2009; Hsin and Qiu 2012; Qiu and Chen 2010;
111 Ren et al. 2020). Given meso-scale eddies mainly extract energy from background flows, the
112 interannual variation of the currents will potentially influence the variation of subthermocline
113 EKE. Therefore, as a continuation of Zhang et al. (2021), this work is aimed to explore the
114 interannual variation of subthermocline EKE east of the Philippine coast with 4 years of mooring
115 measurements and long-term model outputs, and clarify the underlying mechanism and its

116 relationship with ENSO.

117 The rest of the paper is organized as follows. The data and method are presented in Section 2.

118 The interannual variation of subthermocline EKE is described in Section 3. Section 4 shows the

119 governing process of interannual variation of subthermocline EKE. The relationship between

120 subthermocline EKE and ENSO is discussed in Section 5. The conclusion is drawn in Section 6.

121

122 **2. Data and Methodology**

123 **2.1 Data**

124 a. OFES model outputs

125 The interannual variation of subthermocline EKE east of the Philippine coast is investigated

126 based on outputs from the Oceanic General Circulation Model for the Earth Simulator (OFES).

127 The OFES model is based on the third version of the Modular Ocean Model (MOM 3.0) that

128 covers a quasi-global ocean extending from 75°S to 75°N and has a horizontal resolution of 0.1°

129 and 54 vertical levels. The model is first initialized with the World Ocean Atlas 1998 (WOA98)

130 and spun up for 50 years. Driven by different climatological monthly fields, the model produces

131 three types of simulation products, i.e., OFES-CLIM product, which is forced by the same

132 climatological monthly fields of NCEP; OFES-NCEP product, which is integrated from 1950

133 using daily surface wind stress, heat flux, and salinity flux forcing provided by NCEP; and

134 OFES-QSCAT product, which is forced by the wind stress data of the QuikSCAT measurements

135 from 22 July 1999 to 30 October 2009. In this work, the OFES-NCEP outputs with a 3-day

136 snapshot from 1995 to 2017 are used. Detailed descriptions of this model can be found in

137 Masumoto et al. (2004) and Sasaki et al. (2008).

138 OFES outputs have been widely applied to the investigation of the general circulation and
139 meso-scale eddies in the western Pacific, and these studies indicate that the model outputs are
140 generally consistent with different types of observations (e.g., Dutrieux 2009; Wang et al 2014;
141 Chiang and Qu 2013; Song et al. 2017; Zhang et al. 2021). For instance, Song et al. (2017) has
142 compared the climatological mean circulation simulated by OFES with the World Ocean Atlas
143 2013 and indicates that the model outputs roughly agree with observations in both the upper and
144 intermediate layers. Chiang and Qu (2013) reveal a good consistency between the
145 OFES-simulated velocity and mooring observations at 2.5°S, 142°E on the seasonal time scale.
146 Zhang et al. (2021) further compares the modeled subthermocline EKE with three mooring
147 observations east of the Philippines and suggests that the model outputs well capture the seasonal
148 variability of subthermocline EKE recorded by mooring observations. Therefore, we believe that
149 OFES is one of the most suitable model products to explore the ocean currents and meso-scale
150 eddies in the western tropical Pacific.

151 b. Mooring measurements

152 Two subsurface moorings were deployed at 8.5°N, 130°E from 26th September 2015 to 24th
153 October 2019 and 12.5°E, 130°N from 26th December 2016 to 30th November 2018, respectively.
154 One upward-looking and one downward-looking ADCPs were mounted on the main float at 450
155 m for each mooring, which collected nearly 4-year and 2-year velocity data in the upper 900 m,
156 respectively. The original hourly data is daily averaged to remove the tidal influence and then
157 interpolated onto the standard pressure levels from 50 m to 900 m with the vertical interval of 10
158 m. These two moorings are maintained every year to recover data and replace batteries. Due to
159 technical problems, the velocity data at 8.5°N, 130°E from 21th September 2018 to 6th December

160 2018 is unavailable. For detailed configuration of the ADCPs, see Zhang et al. (2014).

161 c. Sea Surface Height

162 The monthly gridded and merged absolute dynamic topography in the tropical Pacific, with a
163 horizontal resolution of $0.25^\circ \times 0.25^\circ$ for the period of 1995-2017 is also used in this study. This
164 dataset is provided by Aviso+ (<http://www.aviso.altimetry.fr>) and distributed by Copernicus
165 Marine Environment Monitoring Service (CMEMS, <http://marine.copernicus.eu/>).

166

167 **2.2 Calculations of EKE and barotropic/baroclinic conversion rate**

168 Previous studies reveal that the dominant periods of subthermocline eddies east of the
169 Philippine coast are about 60-120 days (Qu et al. 2012; Zhang et al. 2014). Therefore, a 150-day
170 high-pass filter is applied to the original velocity data to isolate subthermocline eddy signals, and
171 the 150-day low-pass filtered velocity fields are regarded as the low-frequency varying
172 background flow, as shown in formula (1).

$$173 \quad u(x, y, t) = \tilde{u}(x, y, t) + u'(x, y, t) \quad (1)$$

174 \tilde{u} and u' denote the velocity signals with time scales longer and shorter than 150 days,
175 respectively. u' is also used to calculate the EKE with formula (2).

$$176 \quad EKE = \frac{1}{2}(u'^2 + v'^2) \quad (2)$$

177 The barotropic energy conversion rate (BTR) and baroclinic energy conversion rate (BCR) are
178 usually used to quantify the barotropic and baroclinic instability of the background currents.
179 Positive BTR denotes the transportation of energy from the mean kinetic energy to EKE, and
180 positive BCR means that mesoscale eddies extract energy from the mean available potential
181 energy of the background currents. Many previous studies have revealed the significance of

182 background instability on the generation of subthermocline eddies in the western Pacific (e.g.
 183 Wang et al. 2014; Chiang et al. 2015; Qiu et al. 2015). Thus, BTR and BCR are calculated in this
 184 study according to formula (3) and (4).

$$BTR = -\left[\underbrace{u'u' \frac{\partial \tilde{u}}{\partial x} + u'v' \frac{\partial \tilde{u}}{\partial y}}_{u\text{-term}} + \underbrace{u'v' \frac{\partial \tilde{v}}{\partial x} + v'v' \frac{\partial \tilde{v}}{\partial y}}_{v\text{-term}} \right] \quad (3)$$

185

$$BCR = \left(\frac{g}{\rho_0} \rho' w' \right) \quad (4)$$

186

187 ρ' and w' in formula (4) indicate the 150-day high-pass filtered potential density and vertical
 188 velocity, while g and ρ_0 are the gravity constant and background potential density with the
 189 value of 9.807 m/s^2 and 1025 kg/m^3 , respectively.

190

191 3. Interannual variation of subthermocline EKE

192 One of the most pronounced characteristics in the ocean circulation east of the Philippine coast
 193 is the energetic eddy activities and high EKE in the subsurface layer (Fig. 2; e.g., Qu et al. 2012;
 194 Chiang et al. 2015). Measurements from two subsurface moorings in this region indicate that the
 195 subthermocline EKE exhibits distinguished interannual fluctuations (Fig. 3). Elevated
 196 subthermocline EKE exists during March to June of 2016 and April to June of 2019, and quite
 197 weak subthermocline EKE appears during July 2017 to July 2018 at 8.5°N , 130°E (Fig. 3a).
 198 Similar phenomenon is also shown at 12.5°N , 130°E with strong signals during January to
 199 February of 2017 and weak signals during the rest of the observation period (Fig. 3b). To better
 200 understand the interannual variation of subthermocline EKE in this area, OFES outputs will be
 201 used in the following analysis because mooring observations only provide information at a few
 202 sporadic sites. The 3-day subthermocline EKE derived from OFES outputs during 1995-2017 is

203 first averaged into monthly time series, and then an empirical orthogonal function (EOF) analysis
204 is applied to the monthly EKE. Here, 300-700 m is chosen as the subthermocline layer in the
205 calculation of EKE considering the energetic subthermocline eddy activities in this depth range
206 (Fig. 2b; Zhang et al. 2021).

207 Figure 4 shows the first two leading EOF modes and their corresponding time series. The first
208 EOF mode captures 15 % of the total variance and exhibits a nearly in-phase EKE variation in
209 the whole study area, except for a minor inconsistency southeast of Mindanao Island. The signals
210 are mainly concentrated near the western boundary, consistent with the distribution of
211 subthermocline EKE shown in Fig. 2a. The PC1 (primary component) time series almost
212 coincides with the interannual variation of regional mean subthermocline EKE with their
213 correlation of 0.89 (Fig. 4c). Here, the regional mean subthermocline EKE is averaged in the
214 black box (5°-14°N, 125°-130°E) shown in Figure 4a. Therefore, the first EOF mode reveals the
215 variation of subthermocline EKE on the interannual time scale. The second EOF mode accounts
216 for 7.2 % of the total variance and exhibits a dipole-like structure of EKE separated by 10°N. The
217 PC2 time series demonstrates obvious seasonal cycle with peaks in summer and troughs in winter
218 for most of the years. To further confirm this seasonal cycle, a power spectral analysis is applied
219 to PC2, and the spectrum of PC2 peaks at the period of 1 year, which is statistically significant at
220 the 95 % confidence level (not shown). It suggests that the second EOF mode captures the
221 seasonal cycle of subthermocline EKE east of the Philippine coast, agreeing with Zhang et al.
222 (2021). In addition, the first EOF mode (15.0 %) is beyond double of the proportion of variance
223 of the second mode (7.2%), implying the dominant role of the interannual variation of
224 subthermocline EKE in this region.

225 The interannual variation of subthermocline EKE is further compared with the normalized
226 Nino 3.4 index after 1-year running mean from NOAA Earth System Research Laboratory. Time
227 series of regional mean subthermocline EKE shows elevated value during 1997-1998, 2003-2004,
228 2007-2008, 2010-2011, and 2016-2017, which is closely related to the ENSO events (Fig. 4c).
229 Figure 5 shows the lead-lag correlation between the regional mean subthermocline EKE and
230 Nino 3.4 index, and the correlation reaches 0.49 when ENSO leads by 14 months. Checked case
231 by case, almost every El Niño event is followed by an elevation of subthermocline EKE.
232 Therefore, the interannual variation of the subthermocline EKE seems to be modulated by
233 ENSO.

234 Zhang et al. (2021) has reported opposite seasonal cycle of subthermocline EKE at different
235 latitude bands in this region, and we therefore check the interannual variation of subthermocline
236 EKE at different latitudes and their correlation with ENSO (Fig. 6). In general, the EKE at the
237 lower latitude bands lags ENSO by relatively shorter period, and the lagging time varies from
238 about 8 months at lower latitudes to about 16 months at higher latitudes. This lag correlation is
239 also confirmed by two mooring observations at 8.5°N, 130°E and 12.5°N, 130°E. As shown in
240 Figure 3, when the El Niño occurs during 2015-2016, significant subthermocline EKE firstly
241 appears at 8.5°N, 130°E after about 7 months, then the mooring at 12.5°N, 130°E observes
242 elevated EKE after about 15 months. Moreover, the nearly 4 years of mooring observations at
243 8.5°N, 130°E cover two El Niño events, i.e., 15/16 and 18/19 El Niño, and during the second El
244 Niño cycle, the same lag correlation is also detected with EKE lagging El Niño by 6 months. In
245 addition, Nan et al. (2019) also observes elevated subthermocline eddy activities during
246 June-July of 2016 by a mooring system at 8°N, 129°E, which exactly lags the 15/16 El Niño by

247 7-8 months. Above all, multiple mooring measurements suggest that the interannual variation of
248 subthermocline EKE in this region lags the ENSO events by several months.

249

250 **4. Governing process of the interannual variation of subthermocline EKE**

251 **4.1 Barotropic and baroclinic energy conversion**

252 Generally speaking, meso-scale eddies could be generated through either external forcing or
253 internal instability of background flows. Based on different types of model outputs, Dutrieux
254 (2009) suggests that the intermediate meso-scale eddies east of the Philippine coast are intrinsic
255 to the ocean, mainly sourced from mixed vertical and horizontal instability of the local
256 background flows. Besides, many other previous studies also emphasized the essential role of
257 background flow instability in the generation of subsurface meso-scale eddies in this region (e.g.
258 Wang et al. 2014; Chen et al. 2015; Chiang et al. 2015; Zhang et al. 2021). Therefore, both
259 barotropic and baroclinic energy conversion rates (BTR and BCR) are calculated with OFES data.
260 Figure 7a shows the interannual variation of regional mean subthermocline EKE and the sum of
261 BTR and BCR in the black box east of the Philippine coast (5°-14°, 125°-130°E; Fig. 2a). The
262 regional mean BTR plus BCR matches well with the subthermocline EKE and leads the EKE by
263 4 months with a correlation of 0.78, statistically significant at 95 % confidence level (Fig. 7c).
264 This 4-month lag reflects the ocean's internal adjustment period. Similar lead-lag correlations
265 between the flow instability and EKE are also found in the NEC/STCC region (e.g., Qiu 1999).

266 To further quantify the contributions of barotropic and baroclinic instability to the interannual
267 variation of subthermocline EKE, the time series of regional mean subthermocline BTR and
268 BCR are shown in Figure 7b. In terms of the mean state, the averaged value of BCR is 1.55×10^{-9}

269 m^2/s^3 , almost twice as much as that of BTR which is $0.89 \times 10^{-9} \text{ m}^2/\text{s}^3$. It suggests that
270 subthermocline meso-scale eddies could extract energy from both baroclinic and barotropic
271 instability of the background flows, and the baroclinic process is dominant. Although the mean
272 value of BCR is larger than that of BTR, the interannual variation of subthermocline EKE seems
273 to be mainly controlled by BTR except for 2003. The standard deviation of BTR is 0.71×10^{-9}
274 m^2/s^3 , larger than that of BCR of $0.54 \times 10^{-9} \text{ m}^2/\text{s}^3$ (exclude 2003), implying the dominant role of
275 barotropic instability. Meanwhile, almost every peak in the time series of BTR coincides with the
276 elevated EKE, for example, during 1997, 1999, 2007-2008, 2010-2011, and 2015-2016 (Fig.7a
277 and 7b). Therefore, we suggest that the interannual variation of subthermocline EKE is mainly
278 modulated by the evolution of barotropic instability of the background flows, while the
279 baroclinic instability also plays important role in it.

280 It is worth noting that Figure 6 demonstrates the significant lag correlation between the
281 subthermocline EKE and ENSO, and two correlation maxima with value exceeding 0.5 appear
282 near 7°N and 12°N , separated by a correlation minimum at 9°N . This characteristic suggests that
283 there may be different processes controlling the interannual modulation of subthermocline EKE
284 in the northern and southern parts of the region along the Philippine coast. Therefore, the study
285 region is separated into the northern part ($125^\circ\text{-}130^\circ\text{E}$, $9^\circ\text{-}14^\circ\text{N}$) named Box 1 and southern part
286 ($125^\circ\text{-}130^\circ\text{E}$, $5^\circ\text{-}9^\circ\text{N}$) named Box 2 (Fig. 4a). The interannual variation of regional mean
287 subthermocline EKE and corresponding BTR/BCR in Box 1 and Box 2 are shown in Figure 8. In
288 Box 2, the mean value of BTR is $2.16 \times 10^{-9} \text{ m}^2/\text{s}^3$, significantly larger than that of BCR which is
289 $0.90 \times 10^{-9} \text{ m}^2/\text{s}^3$. Meanwhile, the prominent interannual fluctuation of BTR is detected with a
290 standard deviation of $1.55 \times 10^{-9} \text{ m}^2/\text{s}^3$, which is highly correlated with the interannual variation of

291 subthermocline EKE (Fig. 8b). While the variation of BCR on the interannual time scale is
292 relatively indistinctive with a standard deviation of $0.67 \times 10^{-9} \text{ m}^2/\text{s}^3$, and its relationship with the
293 subthermocline EKE is ambiguous as well. In Box 1, although the mean value of BCR
294 ($2.03 \times 10^{-9} \text{ m}^2/\text{s}^3$) is larger than that of BTR (nearly 0), the interannual variation of BTR is almost
295 coherent with the subthermocline EKE except in 2003 (Fig. 8a), and the BTR exhibits
296 distinguished peaks when enhanced subthermocline EKE appears. In hence, the evolution of
297 barotropic instability is the primary reason for the interannual modulation of subthermocline
298 EKE in both Box 1 and Box 2. As for 2003, the elevated subthermocline EKE seems due to the
299 baroclinic instability (Fig. 8a). There is no La Niña occurring after the 02/03 El Niño event, and
300 this abnormal ENSO cycle may be responsible for the elevated EKE in 2003. Detailed physical
301 processes on this issue will be explored in future studies.

302

303 **4.2 Source of barotropic instability**

304 According to formula (3), the BTR consists of two components which are associated with the
305 horizontal derivative of zonal and meridional background flow. We use u-term and v-term to
306 represent the two components of BTR, and further identify the dominant term. Figure 9 shows
307 the horizontal distribution of climatological mean subthermocline BTR and its two components.
308 In the mean BTR, significant signal appears near the western boundary region, especially east of
309 Mindanao where two positive BTR bands exist nearly parallel to the coast (Fig. 9a), which is
310 similar to the distribution of subthermocline EKE (Fig. 2a). Same as the horizontal distribution of
311 BTR, signals in the u-term and v-term also concentrate in the western boundary region. Negative
312 values are dominant in the u-term, with only several positive spots existing sporadically to the

313 east of the Mindanao coast (Fig. 9b). While the v-term is featured with an opposite spatial pattern
314 to that of u-term, with a 2°-width positive jet locating north of 8°N (Fig. 9c). In general, v-term
315 seems to be the dominant component of subthermocline BTR, but the effect of u-term east of the
316 Mindanao coast is not ignorable.

317 To further clarify which component is dominant on the interannual time scale, the interannual
318 time series of regional mean u-term and v-term are shown in Figure 10. As expected, v-term and
319 u-term exhibit almost opposite interannual variations. v-term is positive during the whole period
320 and is the source of barotropic instability in this region, while u-term is negative for most of the
321 period, implying the zonal flow extracts energy from meso-scale eddies. Moreover, the
322 interannual variation of v-term is consistent with that of BTR (Fig. 7b and Fig. 10), suggesting
323 that the v-term is the dominant component in the interannual variation of BTR. It is worth
324 mentioned that the peak time of v-term is not the same as that of BTR, which is probably due to
325 the modulation of u-term.

326 Above analysis indicates that the interannual modulation of BTR is dominated by v-term,
327 which means the evolution of meridional background flow plays a crucial role in the variation of
328 BTR. East of the Philippine coast, the meridional flow is mainly associated with MC, MUC, and
329 HE (Fig. 1). But in the subsurface layer, the MC south of 15°N is very weak, while the MUC and
330 HE seem strong (Fig. 1b). Therefore, only HE and MUC are considered in the following
331 discussion.

332 HE is a quasi-permanent anticyclonic eddy that is sustained by two boundary currents, MC
333 and NGCC, and it is also the origin of NECC (e.g., Wyrтки, 1961; Lukas et al. 1991). Both
334 observation and model results reveal that HE tilts northwestward with increasing depth from 3°N,

335 130°E in the surface to the Mindanao coast at about 750 m, as shown in Figure 1 (e.g., Qu et al.
336 1999; Kashino et al. 1999). Recent studies indicate that the evolution of HE meandering is
337 responsible for the seasonal variation of BTR, which further modulates the EKE variation in both
338 the surface and subsurface layer in this region (Chen et al. 2015; Zhang et al. 2021). Therefore,
339 the interannual evolution of subthermocline BTR east of the Mindanao Island may be also
340 influenced by the subsurface component of HE. To examine the interannual variation of
341 subsurface HE, a box (127°-130.5°E, 3.5°-8°N) is chosen to calculate the time series of regional
342 mean HE vorticity in the subsurface layer (Fig. 11a). The result indicates that the interannual
343 variation of HE vorticity exhibits simultaneous correlation with the BTR, and the correlation
344 reaches 0.53. Same as Chen et al. (2015) and Zhang et al. (2021), the enhancement of HE means
345 increasing nonlinear shears of the background flows, which extracts more energy from the mean
346 kinetic energy to EKE through barotropic instability. Thus, we suggest that the interannual
347 variation of subthermocline BTR east of the Mindanao Island (Box 2 in Fig. 4a) is mainly related
348 to the evolution of HE in the subsurface layer.

349 Further north, the MUC exists below 500 m under the surface MC, which flows northward
350 with a maximum mean velocity around 10 cm/s (Hu and Cui, 1989, 1991). Based on
351 hydrographic data, a time-mean MUC is observed from 6° to 13°N (e.g., Wang and Hu 1998; Qiu
352 et al. 2015). Nevertheless, in the mean subthermocline circulation derived from OFES outputs
353 (Fig. 1b), the northward velocity between 6°-8°N is influenced strongly by the HE. Therefore, the
354 following analysis is focused on the meridional velocity between 8°-13°N to investigate the MUC
355 variations.

356 EOF analysis is applied to the regional mean meridional velocity time series between 8°-13°N

357 from coast to 129°E. Here, the velocity is interpolated onto a regular 20m-depth interval between
358 0-1000 m before the EOF analysis to eliminate the bias caused by irregular vertical grid of model
359 outputs. Figure 12 shows the first two EOF modes and their corresponding PC time series. The
360 first EOF mode captures 69.1 % of the total variance and reveals a surface-intensified pattern that
361 is closely related to MC. Furthermore, the PC1 coincides well with the interannual variation of
362 the MC strength (Fig. 12c), and here the MC strength is defined as the mean velocity from the
363 coast to 129°E between 8°-13°N in the upper 460 m. In hence, the first EOF mode reflects the
364 interannual variation of MC. The second EOF mode exhibits subsurface-intensified features of
365 the meridional velocity and accounts for 20.3 % of the total variance. The corresponding PC2
366 agrees well with the interannual variation of MUC strength whose definition is the same as MC
367 but for the depth range of 460-1000 m (Fig. 12d). Similar EOF results are also obtained based on
368 ORAS4 reanalysis data that has a longer period from 1958 to 2017 (not shown). Meanwhile, the
369 interannual variation of MUC matches well with the BTR v-term with a correlation of 0.47 (Fig.
370 10 and Fig. 12d). Therefore, we suggest that the interannual variation of subthermocline BTR
371 east of the Philippine coast is attributed to the evolution of MUC. When the MUC is strong, the
372 nonlinear shear of subthermocline meridional velocity increases and the background flow is more
373 barotropically unstable, which means more kinetic energy of the background currents is
374 converted into the EKE. It is worth noting that the MUC flows northward from the northern part
375 of Box 2 to Box 1 (8°-13°N, Fig. 1b), exerting significant influences on the subthermocline EKE
376 evolution in both boxes. While the HE exists southeast of Mindanao, and its implication to EKE
377 is mainly in the southern part along the Philippine coast.

378

379 **5. Discussion**

380 Both mooring observations and model results reveal the delayed response of subthermocline
381 EKE to ENSO (Fig. 3 and Fig. 4c). Generally, this kind of delayed oceanic response to ENSO is
382 usually associated with the adjustment through baroclinic Rossby waves (e.g., Qiu and Chen
383 2010; Hsin and Qiu. 2012). Based on the altimeter products, Hsin and Qiu (2012) denotes that
384 the intensity and meridional migration of NECC can be modulated by the westward propagating
385 Rossby wave. As the source region of NECC, HE may be also influenced by Rossby wave. To
386 investigate this impact, the Hovmöller diagrams of sea surface height anomaly (SSHA) between
387 5°-8°N derived from satellite altimetry and OFES outputs are shown in Figure 13. The result
388 indicates that OFES outputs capture the observed characteristics of SSHA on both the annual and
389 interannual time scales, which confirms the capability of OFES in simulating the ocean
390 circulation in the Pacific. On the interannual time scale, when El Niño occurs, positive wind
391 stress curl anomaly (WSCA) near the dateline excites negative SSHA, which propagates
392 westward in the form of the first mode baroclinic Rossby wave, affecting the intensity of HE in a
393 delayed fashion (Fig. 11b and Fig. 13). For example, during the 15/16 El Niño event, the
394 negative SSHA appears near the dateline in August 2015, then propagates westward and arrives
395 to the western boundary in February 2016, which is consistent with the peak time of HE's
396 vorticity during this event (Fig. 11b). Therefore, the vorticity of HE exhibits a lag correlation
397 with Nino3.4 index, and the coefficient reaches 0.54 when the Nino3.4 index leads by 5 months
398 (Fig. 11b). Because the interannual variation of subthermocline EKE in Box 2 is modulated by
399 HE through its barotropic instability, the subthermocline EKE in Box 2 lags Nino3.4 index by 8
400 months (Fig. 6). This 3-month time lag between the HE variation and subthermocline EKE is

401 supposed to be related to the internal adjustment process of the ocean.

402 As for the interannual variation of MUC, there are only a few previous studies due to the lack of
403 long-time subsurface observations (e.g., Hu et al., 2016; Ren et al., 2020). Based on 4-year
404 subsurface mooring measurements and numerical sensitivity experiments, Hu et al. (2016)
405 suggests that Rossby waves generated near the dateline are of much significance in the MUC
406 variation. Moreover, the Rossby waves usually take about one year translating from the dateline
407 to the western boundary in the latitude band of 10°-15°N, which is probably the reason that the
408 MUC and corresponding BTR lag the Nino3.4 index for about one year as shown in Figure 10
409 and Figure 12d. Furthermore, Qiu et al. (2015) has emphasized the role of baroclinic instability
410 in the eddy generation and Figure 7b also demonstrates the significance of baroclinic instability
411 especially during 2003. In hence, although the barotropic instability is dominant in the
412 interannual variation of subthermocline EKE, the baroclinic instability also has substantial
413 contributions, and detailed investigations are needed in future research.

414

415 **6. Conclusion**

416 The interannual variation of subthermocline EKE east of the Philippine coast is investigated
417 based on 4-year mooring observations during 2015-2019 and OFES outputs during 1995-2017.
418 The results indicate that the interannual variation of subthermocline EKE is closely related to
419 ENSO. Generally, elevated subthermocline EKE appears after El Niño events, and the correlation
420 between EKE and Nino3.4 index is 0.49 when Nino3.4 index leads by 14 months. Nevertheless,
421 such correlation is not latitudinally uniform: low-latitude subthermocline EKE between 5°-9°N
422 lags Nino3.4 index by about 8 months, while the delay is 16 months in relatively higher latitudes

423 between 9°-14°N. Mooring measurements at 8.5°N, 130°E and 12.5°N, 130°E also confirm this
424 delayed response. Further investigations imply that the background flow instability including
425 baroclinic and barotropic instability plays an essential role in the interannual modulation of
426 subthermocline EKE, and the barotropic instability is dominant. Furthermore, the barotropic
427 instability is associated with different background currents. In the southern part of the region east
428 of the Philippines, it is in connection with the subsurface component of the quasi-permanent
429 anticyclonic eddy HE. In the northern part, it is closely related to the MUC. Both MUC and HE
430 are modulated by the westward propagating first mode baroclinic Rossby wave excited by the
431 wind stress curl anomalies near the dateline during ENSO events. Therefore, the subthermocline
432 EKE lags the Nino3.4 index, and subthermocline EKE in the southern part responds faster to
433 ENSO than that in the northern part due to the increasing phase speed of the Rossby wave in the
434 lower-latitude region.

435

436 **Acknowledgments**

437 The authors are grateful to Dr. Cesar Villanoy for helping to recover mooring data. This study
438 is supported by the National Natural Science Foundation of China (No.41776021 and 42122041),
439 the Strategic Priority Research Program of the Chinese Academy of Sciences (No.
440 XDB42010105), the National Key Research and Development Program of China
441 (No.2020YFA0608801 and 2017YFA0603202).

442

443 **Data Availability Statement**

444 The mooring ADCP data is available at the NPOCE website (<http://npoce.qdio.ac.cn/moored>),
445 and OFES data is downloaded from the Asia Pacific Data Research Center (APDRC) website.

446 **Reference**

- 447 Assassi, C., Y. Morel, F. Vandermeirsch, A. Chaigneau, C. Pegliasco, et al., 2016: An Index
448 Distinguish Surface- and Subsurface-Intensified Vortices from Surface Observations. *J. Phys.*
449 *Oceanogr.*, 46: 2529-2552, <http://doi.org/10.1175/JPO-D-15-0122.1>.
- 450 Chelton, D. B., P. Gaube, M. G. Schlax, J. J. Early, and R. M. Samelson, 2011a: The influence of
451 nonlinear mesoscale eddies on near-surface chlorophyll, *Science*, 334, 328–332.
452 <http://doi.org/10.1126/science.1208897>
- 453 Chelton, D. B., M. G. Schlax, R. M. Samelson, 2011b: Global observations of nonlinear mesoscale
454 eddies, *Prog. Oceanogr.*, 91, 167-216, <http://doi.org/10.1016/j.pocean.2011.01.002>
- 455 Chen, X., B. Qiu, S. M. Chen, Y. Q. Qi, and Y. Du, 2015: Seasonal eddy kinetic energy
456 modulations along the North Equatorial Countercurrent in the western Pacific. *J. Geophys.*
457 *Res. Oceans.*, 120, 6351–6362, <https://doi.org/10.1002/2015JC011054>.
- 458 Chiang, T. -L., and T. D. Qu, 2013: Subthermocline eddies in the western equatorial Pacific as
459 shown by an eddy-resolving OGCM. *J. Phys. Oceanogr.*, 43, 1241–1253,
460 <https://doi.org/10.1175/JPO-D-12-0187.1>.
- 461 Chiang, T. -L., C. R. Wu, T. D. Qu, and Y. C. Hsin, 2015: Activities of 50–80 day subthermocline
462 eddies near the Philippine coast. *J. Geophys. Res. Oceans.*, 120, 3606–3623,
463 <https://doi.org/10.1002/2013JC009626>
- 464 Dutrieux, P., 2009: Tropical western Pacific currents and the origin of intraseasonal variability
465 below the thermocline. Ph.D. thesis, University of Hawaii at Manoa, 140 pp.
- 466 Faghmous J. H., I. Frenger, Y. Yao, R. Warmka, A. Lindell, et al., 2015: A daily global mesoscale
467 ocean eddy dataset from satellite altimetry. *Sci Data*, 2:150028.

468 <http://doi.org/10.1038/sdata.2015.28>

469 Firing, E., Y. Kashino, and P. Hacker, 2005: Energetic subthermocline currents observed east of
470 Mindanao. *Deep-Sea Res. II*, 52, 605–613, <https://doi.org/10.1016/j.dsr2.2004.12.007>.

471 Fu, L. -L., 2009: Pattern and velocity of propagation of the global ocean eddy variability, *J.*
472 *Geophys. Res.*, 114, C11017, <http://doi.org/10.1029/2009JC005349>.

473 Hsin, Y. -C., and B. Qiu, 2012: Seasonal fluctuations of the surface North Equatorial
474 Countercurrent (NECC) across the Pacific basin, *J. Geophys. Res.*, 117, C06001,
475 <https://doi.org/10.1029/2011JC007794>

476 Hu D. X. and Coauthors, 2020: Review on observational studies of western tropical Pacific Ocean
477 circulation and climate. *J. Ocean. Limnol.*, 38, 906–929,
478 <https://doi.org/10.1007/s00343-020-0240-1>.

479 Hu, D. X., and M. C. Cui, 1989: The western boundary current in the far-western Pacific Ocean, *in*
480 *Proceedings of Western International Meeting and Workshop on TOGA COARE*, edited by J.
481 Picaut, R. Lukas, and T. Delcroix, pp. 123–134, Inst. Fr. de Rech. Sci. pour le Deev. en Coop.,
482 Noumeea.

483 Hu, D. X., and M. C. Cui, 1991: The western boundary current of the Pacific and its role in the
484 climate. *Chin. J. Oceanol. Limnol.*, 9, 1–14, <https://doi.org/10.1007/BF02849784>.

485 Hu, D., and Coauthors, 2015: Pacific western boundary currents and their roles in climate. *Nature*,
486 522(7556), 299–308. <https://doi.org/10.1038/nature14504>

487 Hu, S. J., D. X. Hu, C. Guan, F. Wang, L. L. Zhang, F. J. Wang and Q. Y. Wang, 2016:
488 Interannual Variability of the Mindanao Current/Undercurrent in Direct Observations and
489 Numerical Simulations. *J. Phys. Oceanogr.*, 46 641 (2), 483-499.

490 <http://doi.org/10.1175/jpo-d-15-0092.1>.

491 Johnson, G. C., and K. E. McTaggart, 2010: Equatorial Pacific 13°C Water eddies in the eastern
492 subtropical South Pacific Ocean. *J. Phys. Oceanogr.*, 40, 226–236.
493 <https://doi.org/10.1175/2009JPO4287.1>

494 Kashino, Y., H. Watanabe, B. Herunadi, M. Aoyama, and D. Hartoyo, 1999: Current variability at
495 the Pacific entrance of the Indonesian throughflow. *J. Geophys. Res.*, 104, 11021–11035,
496 <https://doi.org/10.1029/1999JC900033>

497 Kashino, Y., N. Espana, F. Syamsudin, K. Richards, T. Jensen, P. Dutrieux, and A. Ishida, 2009:
498 Observations of the North Equatorial Current, Mindanao Current, and Kuroshio Current
499 System during the 2006/07 El Niño and 2007/08 La Niña, *J. Oceanogr.*, 65(3), 325–333,
500 <http://doi.org/10.1007/s10872-009-0030-z>.

501 Lukas, R., E. Firing, P. Hacker, P. L. Richardson, C. A. Collins, R. Fine, and R. Gammon, 1991:
502 Observations of the Mindanao Current during the Western Equatorial Pacific Ocean
503 Circulation Study, *J. Geophys. Res.*, 96(C4), 7089–7104, <http://doi.org/10.1029/91JC00062>

504 Lukas, R., T. Yamagata, and J. P. McCreary, 1996: Pacific low latitude western boundary currents
505 and the Indonesian throughflow. *J. Geophys. Res.*, 101, 12209–12216,
506 <https://doi.org/10.1029/96JC01204>.

507 Masumoto, Y., and Coauthors, 2004: A fifty-year eddy resolving simulation of the world
508 ocean—Preliminary outcomes of OFES (OGCM for the Earth Simulator), *J. Earth Simul.*, 1,
509 35–56.

510 McWilliams, J. C., 1985: Submesoscale coherent vortices in the ocean, *Rev. Geophys.*, 23,
511 165–182, <http://doi.org/10.1029/RG023i002p00165>

512 Nan, F., F. Yu, C. J. Wei, Q. Ren, and C. H. Fan, 2017: Observations of an extra-large subsurface
513 anticyclonic eddy in the northwestern Pacific subtropical gyre. *J. Mar. Sci. Res. Dev.*, 7, 235,
514 <https://doi.org/10.4172/2155-9910.1000234>.

515 Nan, F., F. Yu, Q. Ren, C. J. Wei, Y. S. Liu, and S. H. Sun, 2019: Isopycnal mixing of
516 interhemispheric intermediate waters by subthermocline eddies east of the Philippines. *Sci.*
517 *Rep.*, 9, 2957, <http://doi.org/10.1038/s41598-019-39596-2>

518 Nitani, H., 1972: Beginning of the Kuroshio. In H. Stommel, and K. Yoshida (Eds.), Kuroshio:
519 Physical aspects of the Japan current (pp. 129-163). Seattle, WA: University of Washington
520 Press.

521 Qiu, B., 1999: Seasonal eddy field modulation of the North Pacific Subtropical Countercurrent:
522 TOPEX/Poseidon observations and theory. *J. Phys. Oceanogr.*, 29, 2471–2486,
523 [https://doi.org/10.1175/1520-0485\(1999\)029,2471:SEFMOT.2.0.CO;2](https://doi.org/10.1175/1520-0485(1999)029,2471:SEFMOT.2.0.CO;2).

524 Qiu, B., and S. M. Chen, 2010: Interannual-to-decadal variability in the bifurcation of the North
525 Equatorial Current off the Philippines. *J. Phys. Oceanogr.*, 40, 213–225,
526 <http://doi.org/10.1175/2010JPO4462.1>

527 Qiu, B., D. L. Rudnick, S. Chen, and Y. Kashino, 2013: Quasistationary North Equatorial
528 Undercurrent jets across the tropical North Pacific Ocean, *Geophys. Res. Lett.*, 40,
529 2183–2187, <http://doi.org/10.1002/grl.50394>.

530 Qiu, B., S. M. Chen, D. L. Rudnick and Y. J. Kashino, 2015: A New Paradigm for the North
531 Pacific Subthermocline Low-Latitude Western Boundary Current System, *J. Phys.*
532 *Oceanogr.*, 45, 2407-2423, <http://doi.org/10.1175/JPO-D-15-0035.1>

533 Qu T. D., H. Mitsudera, and T. Yamagata, 1999: A climatology of the circulation and water mass

534 distribution near the Philippine coast. *J. Phys. Oceanogr.*, 29, 1488–1505,
535 [https://doi.org/10.1175/1520-0485\(1999\)029,1488:ACOTCA.2.0.CO;2](https://doi.org/10.1175/1520-0485(1999)029,1488:ACOTCA.2.0.CO;2).

536 Qu T. D., T. L. Chiang, C. R. Wu, P. Dutrieux, and D. X. Hu, 2012: Mindanao
537 current/undercurrent in an eddy-resolving GCM. *J. Geophys. Res.*, 117, C06026,
538 <https://doi.org/10.1029/2011JC007838>.

539 Ren Q. P., Y. L. Li, F. Wang, J. Duan, S. J. Hu, and F. J. Wang, 2020: Variability of the Mindanao
540 Current Induced by El Niño Events, *J. Phys. Oceanogr.*,
541 <http://doi.org/10.1175/JPO-D-19-0150.1>.

542 Richardson, P. L., A. S. Bower, and W. Zenk, 2000: A census of Meddies tracked by floats. *Prog.*
543 *Oceanogr.*, 45, 209–250, [http://doi.org/10.1016/S0079-6611\(99\)00053-1](http://doi.org/10.1016/S0079-6611(99)00053-1).

544 Sasaki, H., M. Nonaka, Y. Masumoto, Y. Sasai, H. Uehara, and H. Sakuma, 2008: An
545 eddy-resolving hindcast simulation of the quasiglobal ocean from 1950 to 2003 on the Earth
546 Simulator, *High Resolution Numerical Modeling of the Atmosphere and Ocean*, K. Hamilton
547 and W. Ohfuchi, Eds. Springer, 57–185, http://doi.org/10.1007/978-0-387-49791-4_10.

548 Shapiro, G. I., and S. L. Meschanov, 1991: Distribution and spreading of Red Sea Water and salt
549 lens formation in the northwest Indian Ocean. *Deep-Sea Res.*, 38A, 21–34,
550 [http://doi.org/10.1016/0198-0149\(91\)90052-H](http://doi.org/10.1016/0198-0149(91)90052-H).

551 Simpson, J. J., and R. J. Lynn, 1990: A mesoscale eddy dipole in the offshore California Current. *J.*
552 *Geophys. Res.*, 95 (C8), 13 009–13 022. <https://doi.org/10.1029/JC095iC08p13009>

553 Song L. N., Y. L. Li, C. Y. Liu, and F. Wang, 2016: Subthermocline anticyclonic gyre east of
554 Mindanao and its relationship with the Mindanao Undercurrent, *Chinese Journal of*
555 *Oceanology and Limnology*, 35(6), 1303-1318, <https://doi.org/10.1007/s00343-017-6111-8>

556 Stammer, D., 1998: On eddy characteristics, eddy transports, and mean flow properties, *J. Phys.*
557 *Oceanogr.*, 28, 727–739.
558 [http://doi.org/10.1175/1520-0485\(1998\)028<0727:OECETA>2.0.CO;2](http://doi.org/10.1175/1520-0485(1998)028<0727:OECETA>2.0.CO;2)

559 Toole, J. M., R. C. Millard, Z. Wang, and S. Pu, 1990: Observations of the Pacific North
560 Equatorial Current Bifurcation at the Philippine Coast. *J. Phys. Oceanogr.* 20, 307-318,
561 [http://doi.org/10.1175/1520-0485\(1990\)020<0307:OOTPNE>2.0.CO;2](http://doi.org/10.1175/1520-0485(1990)020<0307:OOTPNE>2.0.CO;2).

562 Wang F, Zang N, Li Y L, Hu D X. 2015. On the subsurface countercurrents in the Philippine Sea.
563 *J. Geophys. Res. Oceans*, 120 (1): 131-144.

564 Wang, F., and D. X. Hu, 1998: Dynamic and thermohaline properties of the Mindanao
565 undercurrent, part I: Dynamic structure, *Chin. J. Oceanol.*, 16(2):122-127,
566 <http://doi.org/10.1007/BF02845177>

567 Wang, Q. Y., F. G. Zhai, F. J. Wang, and D. X. Hu, 2014: Intraseasonal variability of the
568 subthermocline current east of Mindanao. *J. Geophys. Res. Oceans*, 119, 8552–8566,
569 <https://doi.org/10.1002/2014JC010343>.

570 Wyrтки, K., 1961: Physical oceanography of the southeast Asian waters. NAGA Rep. 2, Scripps
571 Institution of Oceanography, 195 pp., <https://escholarship.org/uc/item/49n9x3t4>.

572 Xu, A. Q., F. Yu, and F. Nan, 2019: Study of subsurface eddy properties in northwestern Pacific
573 Ocean based on an eddy-resolving OGCM. *Ocean. Dyn.*, 69, 463–474,
574 <https://doi.org/10.1007/s10236-019-01255-5>.

575 Yuan, D., Z. Zhang, P. C. Chu, and W. K. Dewar, 2014: Geostrophic circulation in the tropical
576 north Pacific Ocean based on Argo profiles. *J. Phys. Oceanogr.*, 44, 558–575,
577 <https://doi.org/10.1175/JPO-D-12-0230.1>.

578 Zhang L. L., Y. C. Hui, T. D. Qu, and D. X. Hu, 2021: Seasonal variability of subthermocline eddy
579 kinetic energy east of the Philippines, *J. Phys. Oceanogr.*,
580 <http://doi.org/10.1175/JPO-D-20-0101.1>.

581 Zhang, L. L., D. X. Hu, S. J. Hu, F. Wang, F. J. Wang, and D. L. Yuan, 2014: Mindanao
582 Current/Undercurrent measured by a subsurface mooring,. *J. Geophys. Res.*, 119, 3617–3628,
583 <https://doi.org/10.1002/2013JC009693>.

584

585

586

587

588

589

590

591

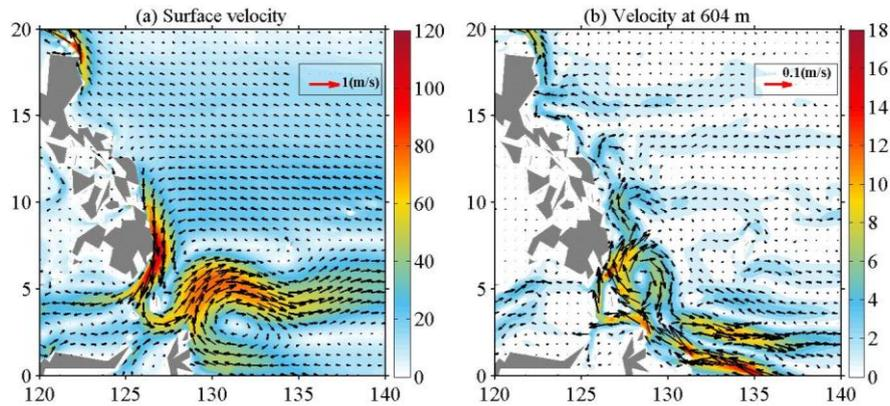
592

593

594

595

596



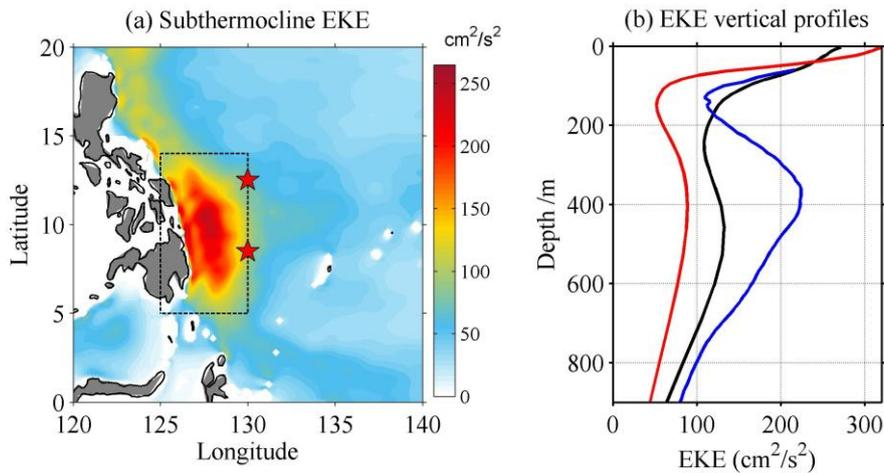
597

598 Fig. 1. (a) Surface (2.5 m) and (b) subsurface (604 m) climatological mean velocity (vectors; m/s)
 599 derived from OFES during 1995 to 2017. Shadings denote the magnitude of the velocity.

600

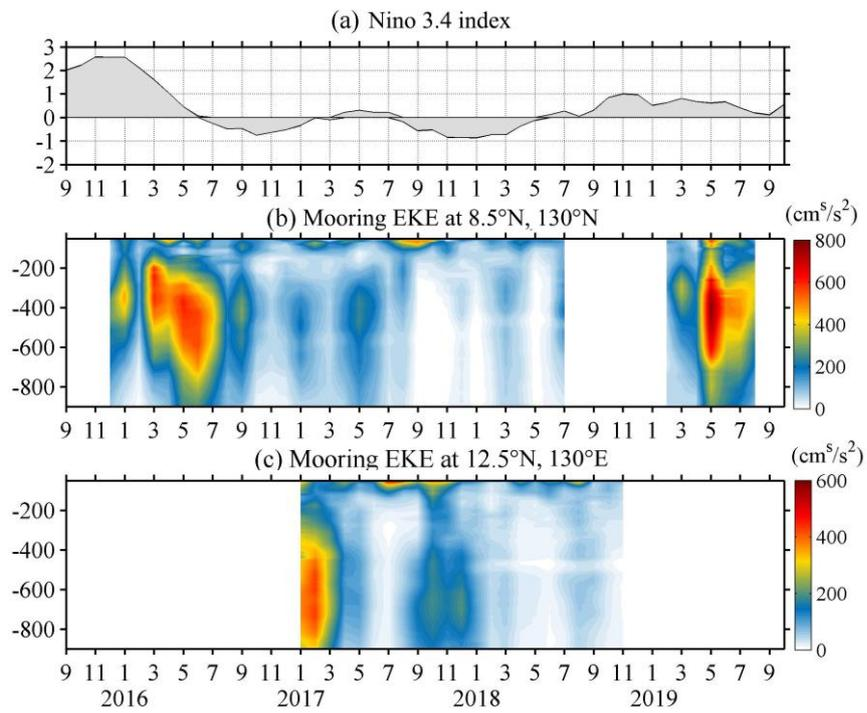
601

602



603

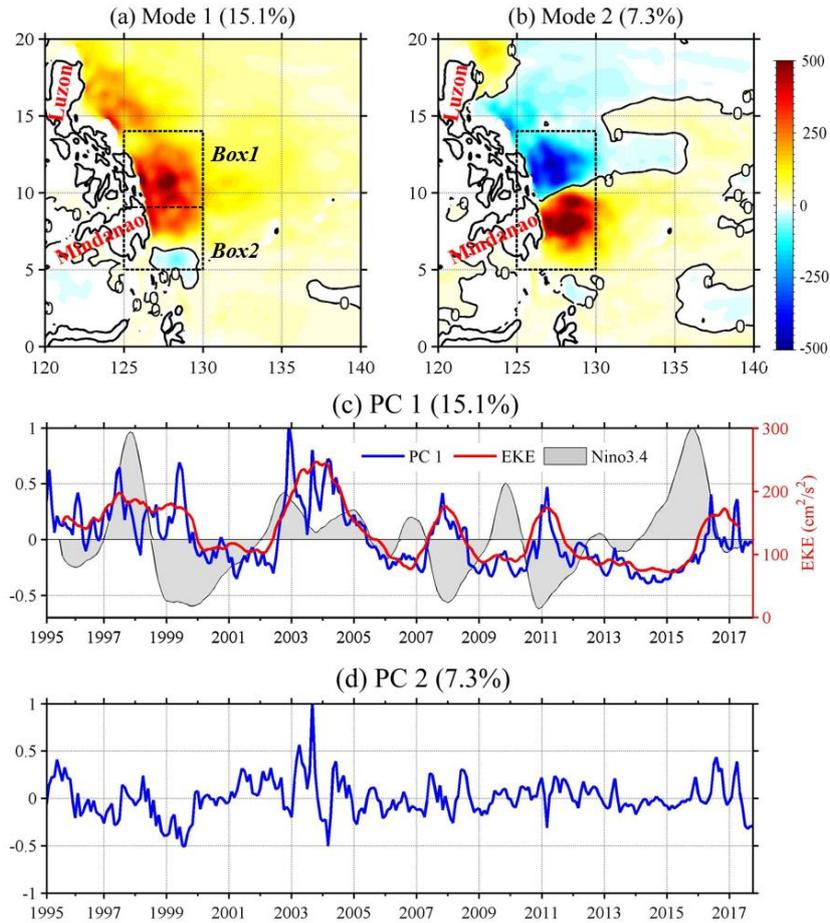
604 Fig. 2. (a) All-time mean subthermocline EKE (300-700 m; cm^2/s^2) calculated with 150-day
 605 high-pass-filtered velocity from OFES during 1995-2017. (b) EKE profiles calculated with
 606 velocity from OFES (red) and mooring ADCP (blue) at 8.5°N, 130°E during December 2015 to
 607 August 2019, and the regional (125°-130°E, 5°-14°N) mean profile calculated with OFES during
 608 1995-2017 (black). Red stars in (a) indicate the mooring locations at 8.5°N, 130°E and
 609 12.5°N, 130°E.



610

611 Fig. 3. (a) Nino 3.4 index, and monthly time series of EKE (color) derived from mooring

612 measurements at (b) 8.5°N, 130°E and (c) 12.5°N, 130°E during September 2015 to October 2019.

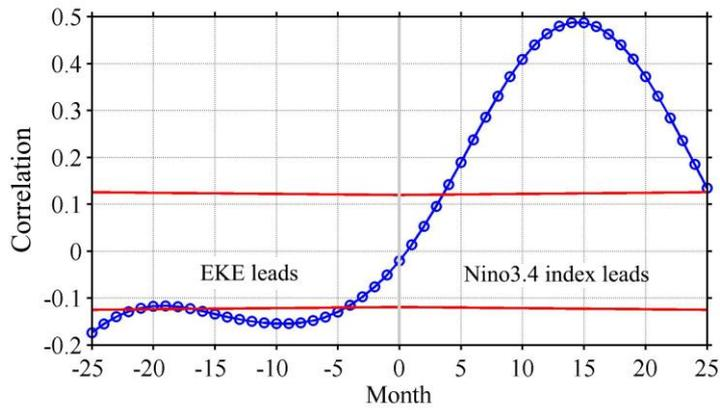


613

614 Fig. 4. (a) Spatial pattern and (c) primary component of the first EOF mode of monthly
 615 subthermocline EKE (300-700 m) in the western Pacific derived from OFES during 1995 to 2017.

616 (b) and (d) are the same as (a) and (c), but for the second EOF mode. The red curve and grey
 617 shading in (c) are the regional (5°-14°N, 125°-130°E) mean time series of subthermocline EKE and
 618 normalized Nino 3.4 index, respectively, and both curves have been smoothed with a one-year
 619 low-pass filter.

620



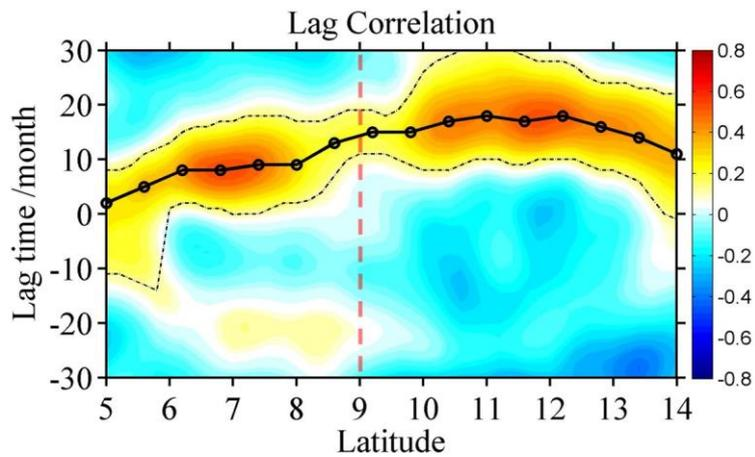
621

622 Fig. 5. Lead-lag correlation between the regional mean subthermocline EKE (red curve in Fig. 4c)

623 and Nino 3.4 index (grey coloring in Fig. 4c). Positive lag means Nino 3.4 index leads the EKE.

624

625



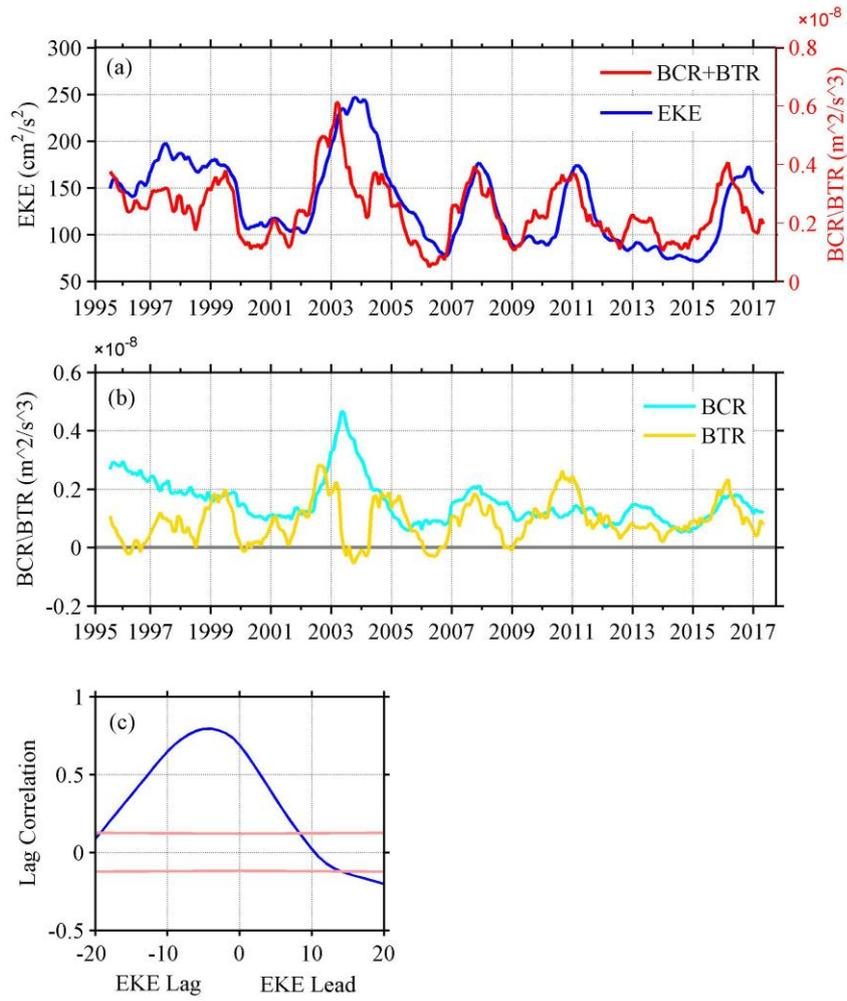
626

627 Fig. 6. Lead-lag correlation between Nino3.4 index and zonal mean (125°-130°E) subthermocline

628 EKE (300-700 m) east of the Philippine coast at different latitudes. Positive lag means Nino 3.4

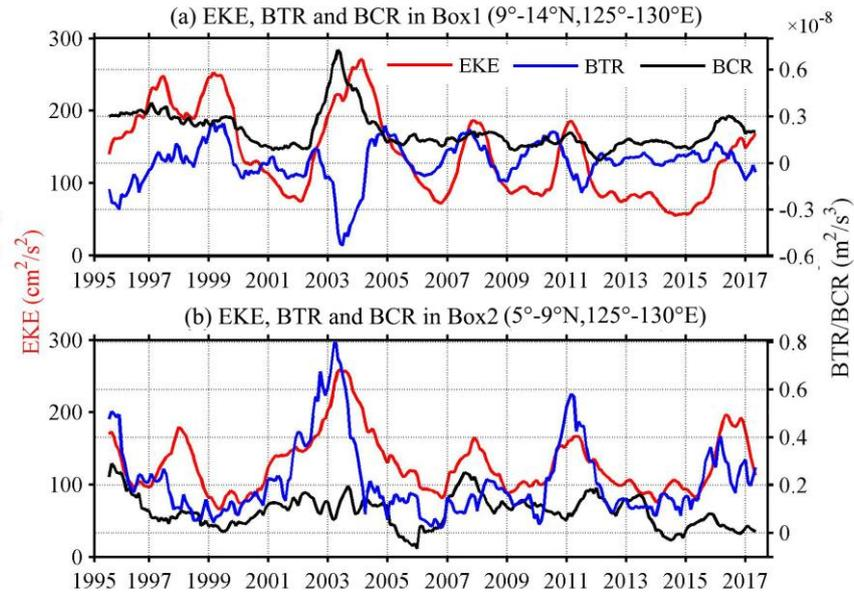
629 index leads the EKE.

630



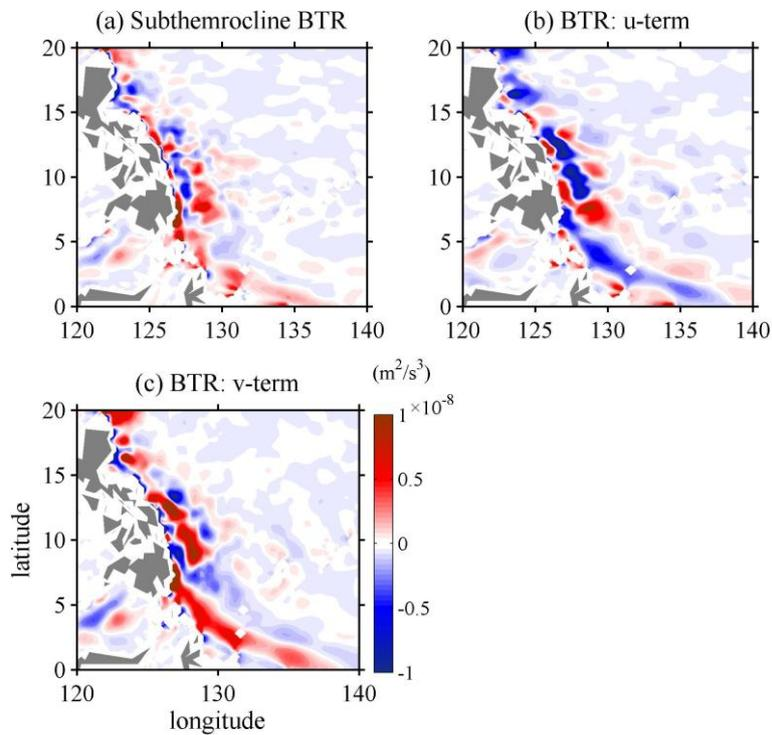
631

632 Fig. 7. (a) Time series of the regional (5° - 14° N, 125° - 130° E) mean subthermocline EKE (red) and
 633 the sum of BTR and BCR (blue). (b) is the same as (a), but for the BTR (yellow) and BCR (light
 634 blue). (c) denotes the lead-lag correlation between the red and blue curves in (a). All the time
 635 series are derived from OFES during 1995-2017 and smoothed with a one-year low-pass filter.



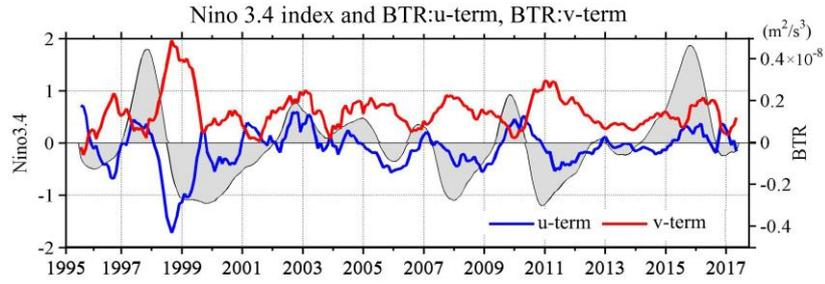
636

637 Fig. 8. (a) Time series of the regional mean subthermocline EKE (red), BTR (blue) and BCR
 638 (black) in Box1 (9°-14°N, 125°-130°E). (b) is the same as (a), but for Box 2 (5°-9°N, 125°-130°E).
 639 All the time series are derived from OFES during 1995-2017 and smoothed with a one-year
 640 low-pass filter.



641

642 Fig. 9. (a) Climatological mean BTR in the subthermocline layer (300–700 m) derived from OFES
 643 during 1995-2017. (b) and (c) are the same as (a), but for the u-term and v-term, respectively.

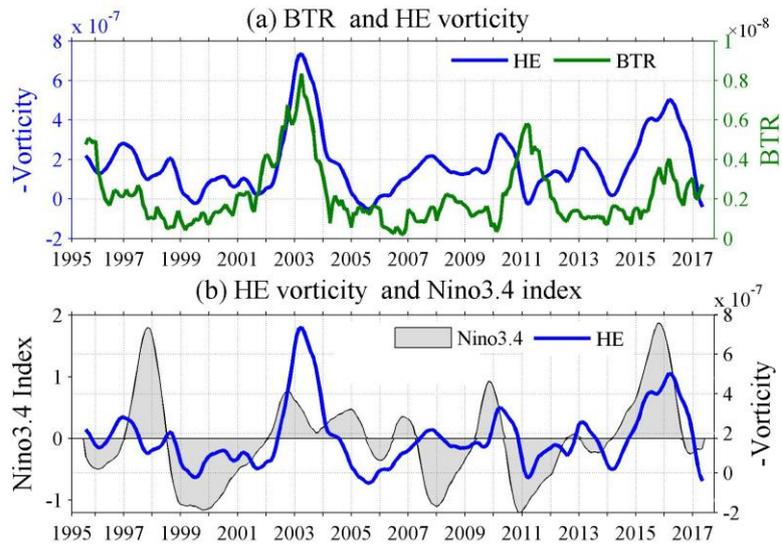


644

645 Fig. 10. Time series of the regional (125°-130°E, 5°-14°N) mean BTR u-term (blue) and v-term
 646 (red) in the subthermocline layer (300-700 m) derived from OFES during 1995-2017. Grey bars
 647 denote the Nino3.4 index. All the time series have been smoothed with a one-year low-pass filter.

648

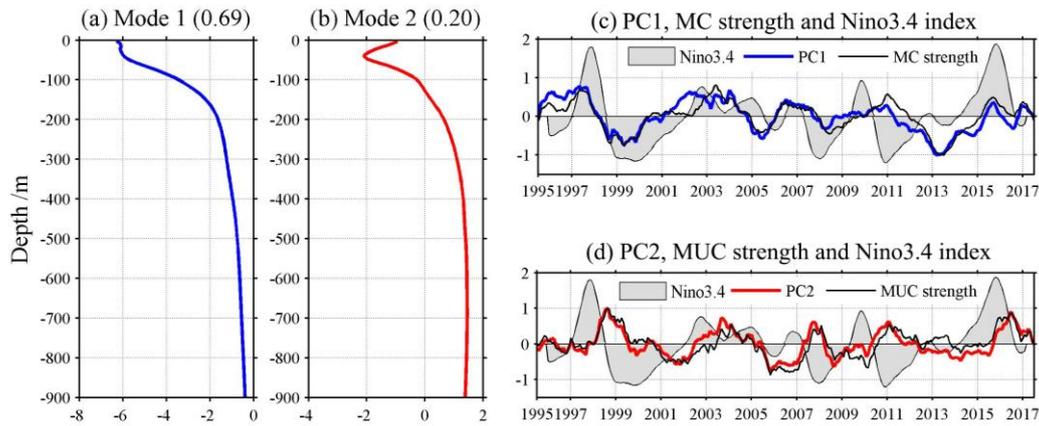
649



650

651 Fig. 11. (a) Time series of the regional mean BTR (green; 5°-9°N, 125°-130°E) and HE vorticity
 652 (blue; 3.5°-8°N, 127°-130.5°E) in the subthermocline layer (300-700 m) derived from OFES
 653 during 1995-2017. (b) Grey bars denote the Nino3.4 index, and blue curve is the same as that in
 654 (a). All the time series have been smoothed with a one-year low-pass filter.

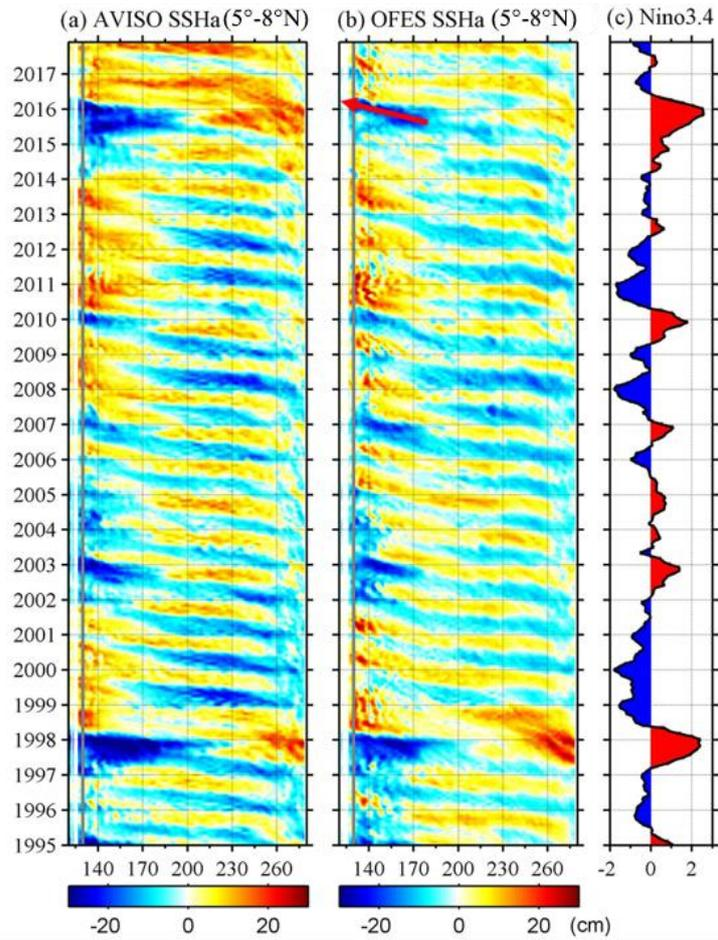
655



656

657 Fig. 12. (a) Vertical profile and (c) primary component of the first EOF mode of monthly
 658 meridional velocity averaged in 8°-13°N, 126°-129°E from OFES during 1995-2017. (b) and (d)
 659 are the same as (a) and (c), but for the second EOF mode. Grey bars in (c) and (d) denote the time
 660 series of Nino 3.4 index. Black curves in (c) and (d) indicate the MC and MUC strength,
 661 respectively. Here the MC strength is defined as the normalized mean velocity from 126°E to
 662 129°E between 8°-13°N in the upper 460 m, and the definition of MUC strength is the same as the
 663 MC, but for the depth range of 460-1000 m.

664



665

666 Fig. 13. Time-longitude plots of monthly sea surface height anomalies averaged between 5°-8°N

667 from (a) satellite altimetry and (b) OFES outputs. (c) Nino 3.4 index.